Effect of the charge-density-wave transition on the thermal expansion of $2H$-$TaSe_2$, $NbSe_3$, and o-TaS_3

D. Maclean and M. H. Jericho
Department of Physics, Dalhousie University, Halifax, Nova Scotia, Canada B3H 3J5
(Received 16 November 1992; revised manuscript received 19 February 1993)

With the help of a tunneling capacitance dilatometer we have measured the thermal expansion near the Peierls temperature (T_C) in three charge-density-wave materials. For the layered compound $2H$-$TaSe_2$, the expansion was measured along the basal plane, while in the trichalcogenides $NbSe_3$ and o-TaS_3 the expansion was measured along the molecular chains. For $2H$-$TaSe_2$ the thermal-expansion coefficient showed a peak with a shape very similar to that reported for the specific heat. In $NbSe_3$ the expansion coefficient showed a discontinuity at T_C, consistent with a mean-field interpretation of the phase transition. For o-TaS_3 the expansion coefficient was measured in the presence of large electric fields. The results suggest a mean-field jump in the expansion coefficient which is of opposite sign to that observed in $NbSe_3$.

I. INTRODUCTION

The charge-density-wave (CDW) state of the transition-metal chalcogenides has been under intensive study in recent years.[1] The quasi-one-dimensional conductors $NbSe_3$ and o-TaS_3 have been of particular interest since their strong non-Ohmic electrical properties have been attributed to the sliding of the CDW with respect to the crystal lattice. Although many aspects of the CDW state in these materials are well understood, others remain problematic. A particularly puzzling observation has been the substantial softening of the dynamic Young's and shear modulus when the samples enter the sliding CDW state.[2] Recent measurements[3,4] of the Young's modulus under near static conditions, however, have revealed no modulus softening even when the samples were taken well into the sliding CDW state. In blue bronze ($K_{0.3}MnO_3$), another quasi-one-dimensional CDW material, the thermal expansion was recently measured by Hauser, Plapp, and Mozurkewich.[5] They reported an 8-K-wide fluctuation region near the Peierls transition and the temperature dependence of the expansion coefficient in this region was consistent with the three-dimensional XY model. In the hope of contributing to a better understanding of the CDW state in general, we have measured the temperature dependence of the thermal expansion of $NbSe_3$ and o-TaS_3 near their CDW onset transitions. The small cross sections of these samples make it difficult to obtain high-resolution measurements of the expansion coefficient with conventional dilatometers and such measurements have not been reported before. In order to perform the dilation measurements under drifting conditions for the CDW, we developed a dilatometer that is based on a tunneling displacement sensor. Section II describes the tunneling dilatometer that was used for the measurements. To test the performance of the dilatometer, the thermal expansion at the CDW onset transition in the layered dichalcogenide $2H$-$TaSe_2$ was measured. The expansion results for all three materials are presented in Sec. III. The results are discussed in Sec. IV, where the expansion measurements are related to other thermodynamic quantities. The results are summarized in Sec. V.

II. EXPERIMENT

A. Tunneling dilatometer

High-resolution thermal-expansion measurements are generally performed with capacitance dilatometers. In such an instrument one plate of the capacitor is fixed, while the other is coupled to the sample and moves in responses to changes in sample length. Samples in a capacitance dilatometer are usually under a small compressive stress. This precludes their use for measurements on mechanically weak samples such as the dichalcogenides and trichalcogenides of this study. An important aspect of this work is the simultaneous measurement of dilation and sample resistance. For these reasons the modified capacitance dilatometer of Fig. 1 was developed.[6] Here absolute length changes are made with a capacitor that has a fixed upper plate and a lower plate in the form of a cantilever. The position of the cantilever is controlled by piezoelectric tubes. The sample support structure consists of a metal frame (c) and a weak cantilever that is fixed to this frame. The samples are stretched between the upper portion of the frame and the end of the cantilever which is deflected upwards or "mechanically biased" in order to keep the sample taut and stretched from end to end. The deflection of the cantilever in response to changes in the sample length is monitored by an electron-tunneling sensor. Electron tunneling is established between a tungsten needle and a small piece of highly oriented pyrolytic graphite (HOPG) mounted on the cantilever. The tunneling current and hence the gap between the needle and the cantilever is kept constant through negative feedback applied to the piezo tubes beneath the movable capacitor plate. In this way sample

0163-1829/93/47(24)/16169(9)/$06.00

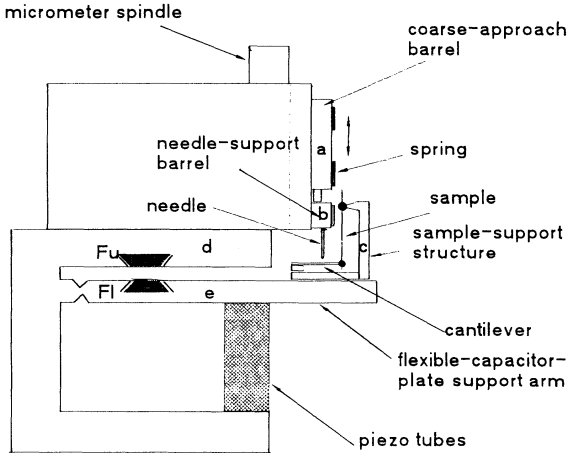

FIG. 1. Schematic arrangement of dilatometer components. The tunneling needle is brought into tunneling range of the graphite surface (not shown) on the cantilever by turning the micrometer spindle. This causes the approach barrel (*a*) and subsequently the needle support barrel (*b*) to move down. Before a measurement commences, barrel (*a*) is pulled back to leave barrel (*b*) behind in its operating position. An electronic feedback signal activates the concentric set of piezo tubes to maintain a constant tunneling current. A change in the sample length results in a change of position of the lower capacitor plate (*Fl*) with respect to the upper plate (*Fu*), and hence a change in the magnitude of the capacitor.

length changes are translated into capacitance changes and the results are not affected by variations in piezo sensitivities. The tunneling needle is mounted in a cylindrical barrel assembly that runs in a *V* groove in the upper capacitor plate structure. In order to establish tunneling a micrometer-activated pin (*a*) pushes the barrel assembly (*b*) and brings the tungsten needle sufficiently close that tunneling can be established when appropriate voltages are applied to the peizo tubes. For temperature-dependent measurements the dilatometer is surrounded by two concentric metal cans. The inner can is filled at room temperature with one atmosphere of helium while the space between the cans is evacuated. The whole system is placed in a standard liquid-nitrogen-precooled set of cryogenic dewars. To minimize the effects of vibrations, the dewar and dilatometer assembly was suspended from the ceiling by elastic cords. Warming of the sample was achieved by a heater wound around the inner can and the temperature was measured with a calibrated semiconducting diode element attached to the upper capacitor structure. Various reproducibility tests showed that the maximum allowable heating (cooling) rate had to be kept below 4.5 K/h. Capacitance variations were measured with an ac capacitance bridge. In terms of length changes, the resolution was 3 Å or one part in 10^7 for the smallest samples used in these experiments. Samples are attached to the sample support structure and to the cantilever with epoxy. For simultaneous electrical measurements four-probe current and voltage leads were attached to the samples outside the epoxied regions. Measurements of the differential sample resistance were made by detecting the ac component of the current through the sample under the influence of an ac voltage excitation which was carried on top of a dc voltage sweep. The differential resistance was then the ratio of the ac voltage amplitude to the detected ac current amplitude. This arrangement allowed the determination of the position and width of any phase transition in the samples. Also, by ramping the dc voltage, studies of the non-Ohmic and threshold field effects in the quasi-one-dimensional CDW compounds could be made.

B. Dilatometer performance

Our main interest in this work was the investigation of the sample length changes in a limited temperature range near phase transitions. Over a limited temperature range reproducible dilatometer calibration could be performed by using copper wires as samples. Over an extended range, however, calibration was not very reproducible. The major source of this irreproducibility was the barrel (*b*) that held the tunneling needle. Since the mobility of this barrel is essential for bringing the tip into tunneling range, it was clamped, with the help of a leaf spring, into a *V* groove in the upper capacitor plate structure. Barrel creep and slippage when the dilatometer temperature was changed over a large range is believed to be responsible for the irreproducibility. Another possible source of difficulty was caused by the fact that the establishment of a tunneling current can be accompanied by a non-negligible force between the needle and the HOPG surface on the cantilever. This is particularly the case when tunneling is established at low temperature where the needle has to penetrate the frozen and insulating contamination layer invariably present on surfaces prepared in air. This did not present a problem for the broader ribbonlike samples such as $2H$-$TaSe_2$. For the threadlike trichalcogenides, however, the tunneling needle could never be positioned on axis with these samples and a small cantilever twist appeared unavoidable. For this reason dilation measurements on the trichalcogenides were performed not by varying dilatometer temperature but by heating the samples directly with an electric current and thus leaving the temperature of all the dilatometer components essentially constant.

C. Samples

All samples were grown by the halogen vapor transport method from metal and chalcogen components that were 99.9999% pure.

III. RESULTS

A. $2H$-$TaSe_2$

To test the overall performance of the dilatometer we measured the expansion of a $2H$-$TaSe_2$ sample. This material shows a transition to a CDW state at 122 K. At this temperature three incommensurate CDW's condense in the basal plane along the three equivalent lattice directions. Below 84 K the three CDW's become commensu-

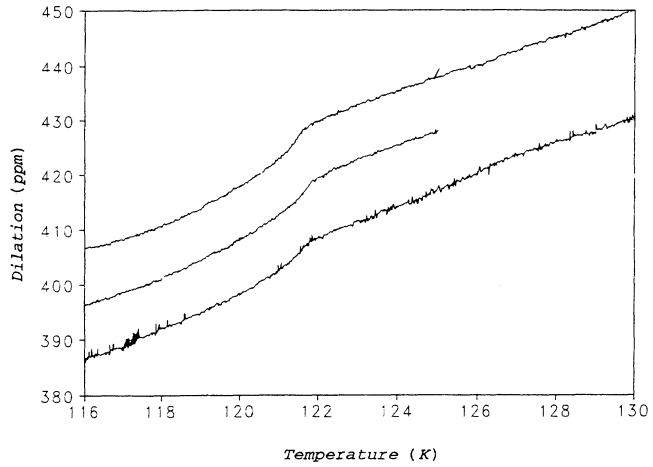

FIG. 2. Raw dilation results for $2H$-$TaSe_2$ near the normal to incommensurate CDW transition. Each curve represents a different temperature sweep. The curves have been offset for clarity.

rate in a first-order transition. High-resolution expansion measurements made near 122 K on a sample with dimensions $2.63\times0.33\times0.07\text{mm}^3$ are shown in Fig. 2. The measurements were made by slowly warming the sample through the transition at 3.6 K/h. The cantilever used was a 0.125-mm-thick phosphor-bronze strip 4.46 mm long and 2.24 mm wide. The mechanical bias applied at room temperature by the deflection of the cantilever resulted in a uniaxial stress of about 9 MPa. Measurements[7] of the hydrostatic pressure dependence of the transition temperature suggest that the above uniaxial stress would shift the transition by at most 0.015 K, well below the 0.02-K resolution of this experiment. For the purpose of a numerical differentiation, data point averaging reduced the temperature resolution to 0.05 K. The three dilation curves shown in Fig. 2 have been arbitrarily offset and represent three separate approaches to tunneling on different parts of the HOPG surface. Possible

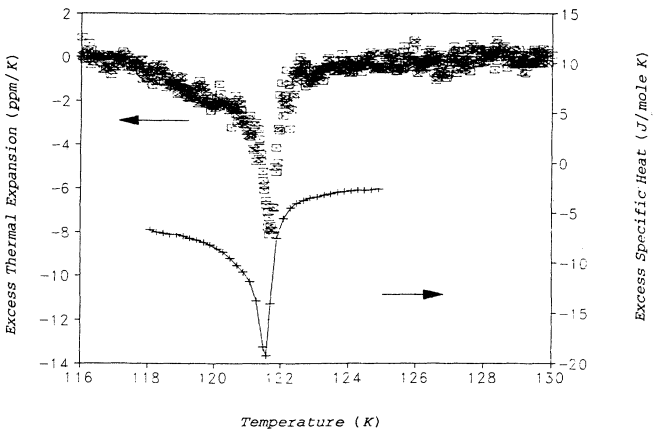

FIG. 3. The upper curve represents the negative of the excess thermal expansion of $2H$-$TaSe_2$. The lower curve represents the excess specific heat as determined by Craven and Meyer (Ref. 9).

lateral movement of the tip over the graphite surface thus did not fold structural features of the graphite surface into the dilation results. An estimation of the dilation discontinuity in the basal plane may be made by linearly extrapolating the sample dilation below 120 K upwards to the transition. This yields a discontinuity of $\Delta a/a=+5.8$ ppm. This value is consistent with the results of Steinitz and Grunzweig-Genossar made by conventional dilatometric methods.[8] Expansion coefficients were calculated from the curves in Fig. 2 by a linear least-squares fit using seven adjacent points. The expansion coefficients for the three curves in Fig. 2 were then averaged to give a single expansion versus temperature curve. The high-temperature behavior of this resultant curve was fitted to a straight line between 124 and 130 K. This line was extended below T_C and the deviation from this line, which represents excess thermal expansion, was calculated.[9] This excess expansion is plotted in Fig. 3.

B. Trichalcogenides

For the reasons discussed above, the thermal expansion of these samples was determined by passing a current through the samples and letting the joule heat raise the sample temperature. A calculation of the temperature distribution in the samples showed that heat loss through the sample ends was negligible and that the sample temperatures were sufficiently uniform for the purposes of this experiment. The reproducibility obtained in such sample self-heating experiments was excellent. The problem with this method is that sample temperature determination becomes difficult. The resistances of the samples are functions of temperature so that in principle they should be able to serve as their own thermometers. However, the non-Ohmic nature of their resistance complicates the temperature determination considerably. The resistance of $NbSe_3$ is sufficiently low so that adequate heating of the samples could be obtained for electric fields below threshold. The samples were temperature cycled starting at 80 K in about 1.5-K increments by raising and subsequently lowering the dc voltage component across the sample such that the threshold field was never exceeded. A field cycle lasted about 6 min, during which the dilatometer temperature drifted upwards by ≈0.3 K. These field cycles were repeated at roughly 3-K intervals. The simultaneous recording of the dc current as well as of the differential resistance permits the determination of the sample resistance and the dissipated power (P). An example of the simultaneously measured resistance and dilation variation for a field cycle is shown in Fig. 4. Outside the negative temperature-coefficient region, i.e., above T_C and below the resistance maximum, the sample temperature can be determined from a calibration in a separate run of sample resistance versus diode sensor temperature. The R versus T and R versus P results can be combined to give the incremental change in the sample temperature with change in power as a function of ambient cell temperature. This is shown in Fig. 5. The data point-free region is the negative temperature-coefficient portion of the $NbSe_3$ resistive behavior. Plotting dT/dP versus $1000(T+67)^{-1}$ tends to result in a

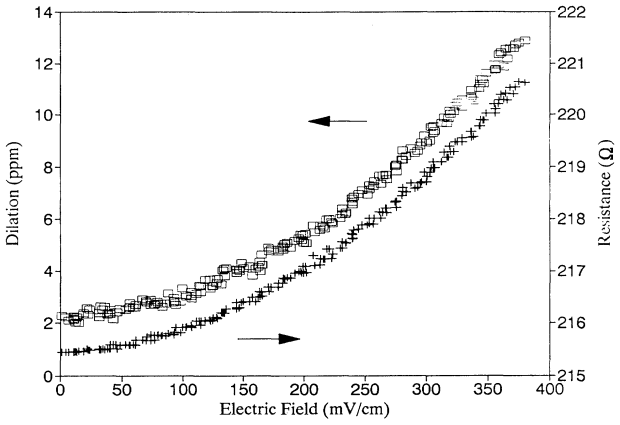

FIG. 4. Electric-field dependence of the dilation and resistance of the $NbSe_3$ sample below threshold. The sample threshold field was 0.5 V/cm and the measurement made at 95.8 K. The observed variation of the resistance and dilation is a consequence of sample heating. The figure includes data gathered with both rising and falling electric field.

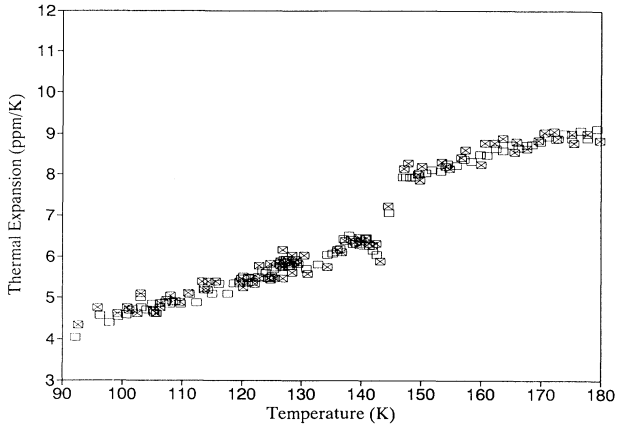

FIG. 6. Thermal expansion of $NbSe_3$ as a function of temperature. The main feature is the jump in the expansion coefficient at the CDW transition. The two symbols correspond to two separate experiments on the same sample.

linear relationship and to determine sample temperatures in this region from power changes; the data portions were extrapolated linearly through the gap region as shown by the solid line in Fig. 5. The results of the expansion coefficient of $NbSe_3$ obtained in this way are shown in Fig. 6 while Fig. 7 shows a high-resolution view of the variation of dilation near the CDW transition region. The expansion measurements in Fig. 6 that were obtained by relating sample temperature to dissipated power agree to within experimental error with those calculated from the resistance-converted temperature outside the negative temperature-coefficient region. A higher-resolution plot of the dilation of $NbSe_3$ near the CDW transition is shown in Fig. 7. In this figure a linear background with a slope of 7.1 ppm/K has been subtracted from the data.

Sample self-heating experiments similar to those performed on $NbSe_3$ were not possible for o-TaS_3. These samples had a much larger resistance and it was not possible to achieve significant heating and still keep the electric field below threshold. The measurements on o-TaS_3 were therefore done by allowing the electric field to exceed the threshold field and the samples were warmed from a low temperature to past the transition temperature in a single heating cycle. Figure 8 shows an example of the measured dilation and the differential resistance as a function of the electric field. Such a field sweep again took about 6 min to complete and since the increasing and decreasing curves nearly overlap, temperature hysteresis effects appear to be negligible. The samples and the helium exchange gas were therefore in thermal equilibrium at each electric-field value. To determine the expansion coefficient it is important to establish a reliable temperature scale. Unlike the measurements on $NbSe_3$, however, a sufficient increase in the temperature of o-

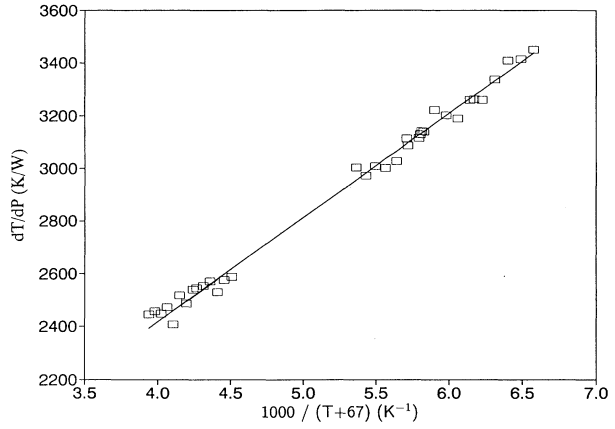

FIG. 5. Change in the sample temperature for a fixed quantity of electrical power as a function of the inverse ambient temperature in $NbSe_3$.

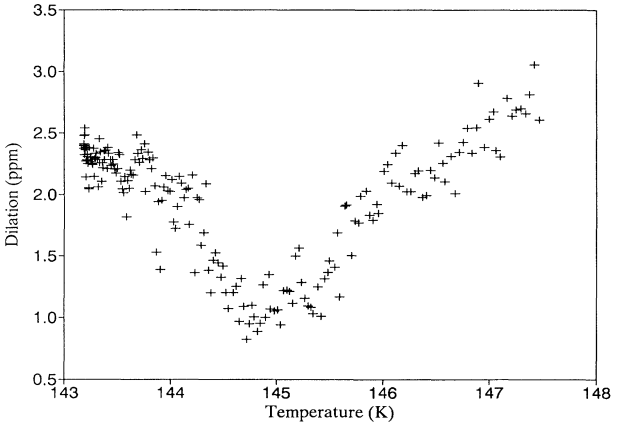

FIG. 7. High-resolution plot of the dilation of $NbSe_3$ as a function of temperature near the CDW phase transition. A linear background with a slope of 7.1 ppm/K has been subtracted from the data.

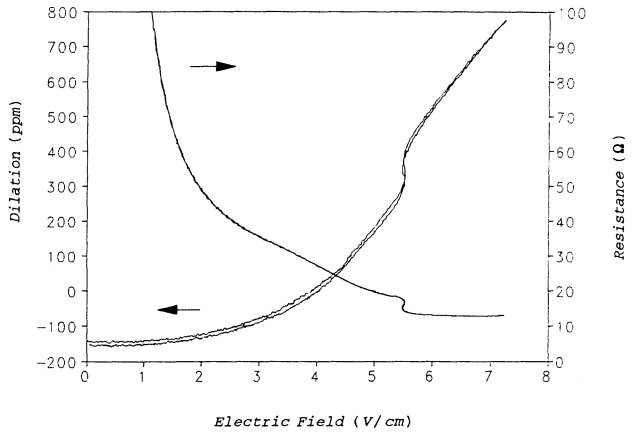

FIG. 8. Dilation and resistance of o-TaS_3 as a function of electric field at 141.1 K. The curves for increasing and decreasing electric field show little evidence of hysteresis.

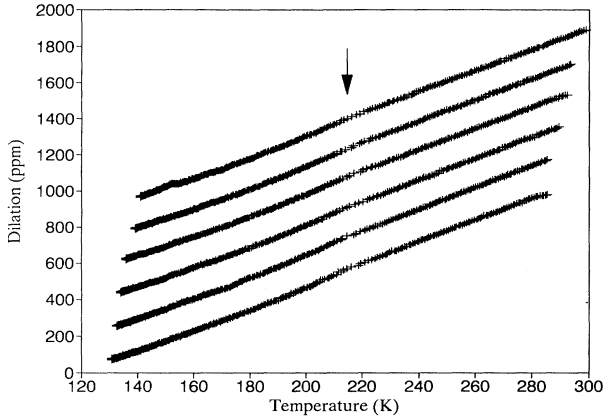

FIG. 9. Temperature dependence of the dilation of an o-TaS_3 sample under a bias strain of 0.09%. The ambient temperature at which the sample self-heating was started increases progressively for the curves shown. The vertical offset between successive curves is arbitrary. The transition temperature T_C is shown by an arrow. The dilation curves above T_C are nearly linear, suggesting a constant expansion coefficient.

TaS_3 samples could only be achieved if the samples were driven well into their non-Ohmic region. In that case the conversion of power into temperature is no longer facilitated by a resistance versus temperature calibration curve and a determination of temperature from dissipated power requires a model for the heat flow from the sample to its surroundings via the helium exchange gas. The functional relationship between sample temperature and power was calculated by taking a concentric arrangement for the sample and surrounding heat sink and then integrating the steady-state heat conduction equation. For a sample of radius a, and a heat sink at radius b, the sample temperature is given by

$$T_S=\left[\left[T_W+\frac{k_0}{k_1}\right]^2-FP\right]^{1/2}-\frac{k_0}{k_1}\ , \tag{1}$$

where the thermal conductivity of the helium gas is given by $K=k_0+k_1T$. T_W is the temperature of the heat sink, P is the dissipated power in the sample of length l, and $F=\ln(a/b)/(4\pi lk_1)$. An examination of the time-dependent heat conduction for a cylindrical geometry showed that the response time for the system was in the millisecond region and the sample and helium must therefore have been in thermal equilibrium during a heating cycle. Equation (1) shows that only for small P or for a temperature-independent thermal conductivity will the sample temperature be proportional to P. The factor F in Eq. (1) was treated as a phenomenological parameter and was determined empirically by measuring P_C, the power needed to reach the CDW transition temperature T_C for different starting temperatures T_W. T_C was identified as the position of the peak in a plot of $-d(\ln R)/dT$ versus T_{Diode} under low power conditions. The power P_C needed to reach the transition temperature was in turn determined from a plot of negative logarithmic derivative of the dc resistance with respect to power. Such a plot shows a distinct peak, the position of which identifies P_C. With F calculated, the conversion of power into temperature may proceed with the help of Eq. (1). The parameter F may exhibit temperature dependence. F was thus calculated separately for each starting temperature and field sweep. Dilation results on o-TaS_3 were also evaluated for the case when heat loss was assumed to be dominated by convection. In that limit dilation curves had lower slopes in the higher-temperature regions and slope changes near T_C were more pronounced than in the conduction-dominated case. An estimate of Grashof and Prandtl numbers suggested that heat loss by convection should have been negligible. We believe that the conduction limit [Eq. (1)] gives a reasonable approximation of the true sample temperature.

The temperature dependence of the dilation for two samples under different states of strain is shown in Figs. 9 and 10. The curves in these figures have been arbitrarily

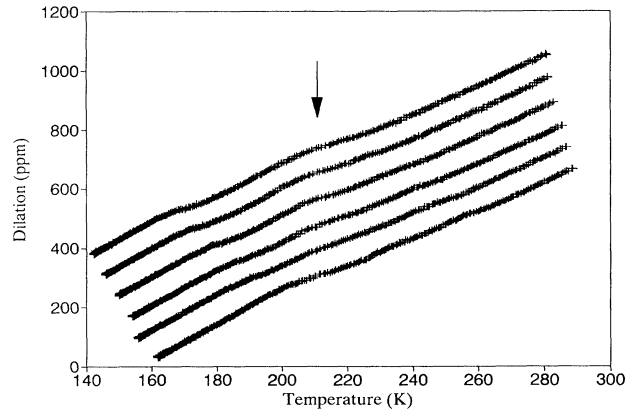

FIG. 10. Temperature dependence of the dilation of an o-TaS_3 sample under a bias strain of 0.18%. Curves represent temperature sweeps at varying starting temperatures. The vertical offset between curves is arbitrary. T_C is marked by an arrow. For starting temperatures below $\sim$163 K a new anomaly appears in the dilation below T_C.

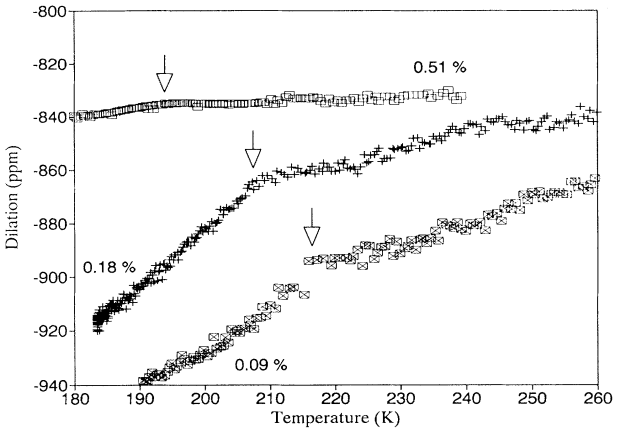

FIG. 11. Temperature dependence of the dilation of o-TaS_3 that was strained at 0.09%, 0.18%, and 0.51%. For the 0.09% and 0.18% strained samples a constant background of 5 ppm/K was subtracted from the data while a background of 4.3 ppm/K was removed from the 0.51% strained sample. Open arrows indicate the transition temperature for each sample.

displaced vertically for clarity. The data represent warming runs with sample warming commencing at progressively higher temperatures. For starting temperatures close to T_C the electric fields in the samples were as low as possible and the results for the dilation under these conditions for three different samples, each under a different bias stress, are shown in Fig. 11. In this figure the detailed behavior near T_C is brought out more clearly by subtracting a background with a constant slope of 5 ppm/K (for the 0.09% and 0.18% strained samples) and 4.3 ppm/K (for the 0.51% strained sample). The temperature scale was derived from Eq. (1) and the starting temperatures for the heating cycles were all close to the CDW onset temperatures. The onset temperatures were obtained from the peaks in the logarithmic derivative of the respective sample resistances. The transition temperatures and electric fields needed to reach T_C for the samples with 0.09%, 0.18%, and 0.51% strains in Fig. 9 were, respectively, 215 K and 4.91 V/cm, 210.5 K and 4.74 V/cm, and 193 K and 4.23 V/cm.

IV. DISCUSSION

A. 2H-$TaSe_2$

From Fig. 3 it is evident that the specific-heat and thermal-expansion data share similar features which suggest a close thermodynamic relationship. The jth component of the uniaxial expansion coefficient at a second-order phase transition is generally discussed with the Testardi relations.[9] In this approach the difference in the Gibbs free energy between the transformed and untransformed phases is written as

$$\Delta G=\phi(\sigma)f\left[\frac{T}{T_C(\sigma)}\right]. \tag{2}$$

Here the order parameter ϕ and the transition temperature T_C are both functions of the stress σ. Testardi showed that the excess thermal expansion is related to the excess specific heat and to the stress derivative of the order parameter by

$$\Delta\alpha_j=-\left[\frac{d\ln T_C}{d\sigma_j}\right]\Delta C_P + \left[\frac{d\ln\phi}{d\sigma_j}-\frac{d\ln T_C}{d\sigma_j}\right]\int_{T_C}^{T}\frac{\Delta C_P(T')}{T'}dT' . \tag{3}$$

The excess in a quantity ΔX is defined as $\Delta X=X^H(T)-X^L(T)$ for all $T<T_C$ where $X^H(T)$ is the observed high-temperature behavior of the system extrapolated to temperatures below T_C while $X^L(T)$ is the actual behavior of the system below T_C. Equation (3) shows that the uniaxial stress dependence of the transition temperature should approximately scale the excess specific heat into the excess uniaxial thermal expansion. The specific heat was obtained from Craven and Meyer.[10] The last term in Eq. (3), which represents the excess entropy, was obtained by means of a numerical integration of the excess specific heat. The transition temperature for the specific-heat measurements differed from the T_C for our samples by 0.88 K. To compare the two sets of data the transition temperature of the specific heat was shifted by this amount. The excess specific heat thus calculated is also shown in Fig. 3. The excess specific-heat curve can be used to determine the excess entropy below T_C. Figure 12 shows a plot $\Delta\alpha/\Delta C_P$ versus $\Delta S/\Delta C_P$. According to Eq. (3) the slope and intercept of this line give $d(\ln T_C)/d\sigma_a=-0.015$ GPa^{-1} and $d(\ln\phi)/d\sigma_a=+0.26$ GPa^{-1}. The logarithmic derivative of the 122-K transition with respect to pressure deduced by Chu *et al.*[7] is $+0.029$ GPa^{-1} while Feldman *et al.*[11] calculated the smaller value of $+0.02$ GPa^{-1}. The a-axis result implies a c-axis stress derivative of between $+0.001$ GPa^{-1} and $+0.010$ GPa^{-1}. The c-axis stress derivative thus may be comparable to the basal-plane stress derivative. If the larger of these two figures is appropriate, then

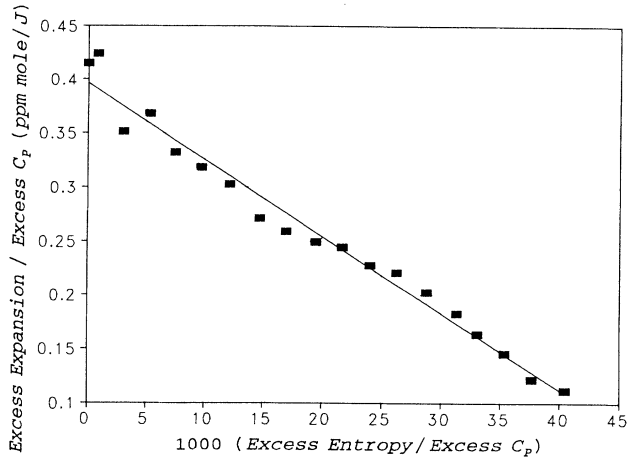

FIG. 12. Plot of the ratio of excess expansion to excess specific heat vs the ratio of excess entropy to excess specific heat for 2H-$TaSe_2$ below the normal to incommensurate CDW transition.

this result would suggest that the interlayer interactions may play a role in the establishment of the CDW state in the material.

An alternative to the above mean-field approach is to recognize that the temperature region near T_C is dominated by fluctuations. The analysis by Craven and Meyer[10] of their specific-heat results showed that the specific heat follows a power law with a critical exponent of 0.45 (± 0.035). Helium atom surface scattering[12] gives an exponent of $\frac{1}{3}$ although the uncertainty is large enough to accommodate an exponent of $\frac{1}{2}$. The uncertainty in our thermal-expansion measurements is considerably larger than that for the specific heat and a meaningful critical exponent analysis could not be made. The results in Fig. 3 are, however, not inconsistent with power-law behavior with exponents in the range of $\frac{1}{2}$ to $\frac{1}{3}$.

B. $NbSe_3$

The results in Fig. 6 show that the expansion coefficient of $NbSe_3$ changes from about 4 ppm/K to 9 ppm/K between 90 and 180 K. At the CDW onset transition the expansion coefficient shows a step discontinuity $\Delta\alpha = 1.8$ (± 0.2) ppm/K. The discontinuity is consistent with the second-order nature of the transition. Fluctuation effects, if present, must be confined to within a few degrees of the transition. It therefore seems appropriate to discuss the transition in terms of the Ehrenfest relations. The specific heat has been measured by Tomic *et al.*[13] and extrapolation of their results about T_C gives a specific-heat discontinuity of $\Delta C_P = +64$ (± 5) kJ/m^3 K. The logarithmic stress derivative of the transition temperature was measured by Lear *et al.*[14] to be -0.031 GPa^{-1}. At T_C these values give a thermal-expansion discontinuity of $\Delta\alpha = +2.0$ ppm/K in close agreement with our measured value. Wang *et al.* have also measured the specific-heat anomaly in $NbSe_3$, finding it to be approximately 8.5 kJ/m^3 K.[15] Our results lend weight to the figure of Tomic *et al.*, but it should be noted that the application of the Ehrenfest relations here depends crucially on the absolute Young's modulus (since Lear *et al.* measure the *strain* derivative of T_C). It has been demonstrated in recent measurements of the Young's modulus in the related material, o-TaS_3, that the static modulus is three to four times smaller than the vibrating-reed measurements.[3,16] If such a reduction of the elastic modulus of $NbSe_3$ were found, then the thermal-expansion results would favor the Wang *et al.* specific-heat anomaly.

Recent results on the quasi-one-dimensional conductor $K_{0.3}MnO_3$ showed clear cusps and hence precursor effects in the expansion coefficient near the CDW onset temperature.[5] These precursor effects were attributed to fluctuations. The critical region was about 8 K wide and the observed temperature dependence was consistent with the three-dimensional XY model. In contrast, our results on $NbSe_3$ only show a mean-field jump, although the resolution of our experiment was not sufficient to permit a clear identification of a precursor region. It is, however, doubtful that the fluctuation-dominated region is more than a few degrees wide.

C. o-TaS_3

The results of Fig. 9 in principle permit a determination of the thermal-expansion coefficient of o-TaS_3 and the change in this coefficient as the sample crosses the transition temperature. The measurements on o-TaS_3, however, were made under an applied stress and in the presence of very large electric fields. These two factors greatly complicate the discussion of the thermal-expansion coefficient. If the Young's modulus of the sample is temperature or field dependent, then an additional sample dilation may be present as a result of the bias stress on the sample. A 1% change in the Young's modulus contributes about 10 ppm to the dilation for the 0.09% strained sample. With the sample kept at a fixed temperature below T_C no electric-field effects on the dilation were ever observed even though a simultaneous measurement of the resistance always showed a clear threshold effect.[4] These results are consistent with the findings of Tritt, Skove, and Ehrlich[3] that, unlike the dynamic modulus, the static modulus does not soften. In a recent examination of the metastable states of o-TaS_3 Hoen *et al.*[17] found length changes associated with the threshold field of between 0.2 ppm and 2.2 ppm, thus appearing to contradict our dilation observations near threshold. However, it is believed that the application of uniaxial stress is the critical factor in the interpretation of these discrepancies. Hoen *et al.* apply very small stresses, typically less than 1 MPa, while the experiments reported here and those of Tritt *et al.* use stresses more than two orders of magnitude larger. It has been shown that the application of uniaxial stress in o-TaS_3 leads to a reduction in the metastable states in this system (and their complete disappearance for strains above 0.5%).[18] It is suggested that the preparation of o-TaS_3 in a low metastable-state condition by uniaxial stress is responsible for these differences. Moreover, it is noted that no hysteretic effects in the resistance were observed in our experiments, in contrast to the observations of Hoen *et al.*

For starting temperatures above 180 K we believe that the main effect of the electric fields in our measurements was to raise the sample temperature through joule heating. In high-quality stress-free samples, a 1% cusp-shaped softening of the dynamic modulus is generally observed.[19,20] The measured dilation should therefore show an increase near T_C that corresponds to this change in the Young's modulus. In principle, the dilation results in Fig. 9 can be corrected for the modulus softening at T_C. It is well known, however, that elastic features often show considerable variability and sample dependence. It is therefore likely that, as a consequence of the applied stresses, the Young's modulus anomalies in our samples were reduced in magnitude and may also have been considerably broadened. To examine the effect of Young's modulus changes near T_C on the dilation curves, the Young's modulus softening was assumed to have the general shape observed in stress-free samples.[19,20] If the dilation results in Fig. 9 are corrected for the full Young's modulus changes usually observed, then new and in our view artificial structure is introduced into the dilation

curves near T_C. This is particularly true for the 0.51% strained sample which develops a deep cusp at T_C which would result in an unreasonable variation of α with temperature. In view of the fact that no electric-field-induced modulus softening has been observed for static conditions, we cannot be certain what form the modulus softening will take near T_C in our samples. The region within ± 10 K of the transition temperature is therefore not accessible to detailed analysis. Outside this region the correction for elastic effects is expected to be smaller and estimates for the expansion coefficient can be attempted. For the 0.18% strained sample between 183 and 195 K the expansion coefficient is 6.8 ppm/K while the value in the 240–260-K region is 5.6 ppm/K. The extrapolated change in the thermal-expansion coefficient at T_C is therefore $\Delta\alpha = -1.2$ ppm/K. For the 0.09% strained sample in the same temperature regimes the expansion coefficient above T_C is 6.1 ppm/K while below T_C it is 5.8 ppm/K, giving $\Delta\alpha = -0.3$ ppm/K. The corresponding change in the expansion coefficient for the 0.51% strained sample, without correcting for modulus changes, is $\Delta\alpha = -0.4$ ppm/K. There is thus a substantial variation in the mean-field jump of the expansion coefficient deduced from our data. If we assume a representative mean-field jump of $\Delta\alpha = -0.7$ ppm/K, then from the stress dependence of T_C one may expect a ΔC_P of -10 kJ/m^3 K or -2.9 kJ/m^3 K depending on whether the dynamic or static Young's modulus is used. Wang *et al.* report that no specific-heat anomaly can be observed in *o*-TaS_3 above a minimum resolution of $0.03R_0$ or 5.3 kJ/m^3 K.[15] Therefore, our thermal-expansion measurements appear to be consistent with the specific-heat measurements. In view of the presence of both large uniaxial stresses and high electric fields in these samples, such a conclusion must be viewed with reservation.

The results in Fig. 10 for the sample under 0.18% strain are particularly puzzling. The results show that as the starting temperature for sample warmup decreases, a hump develops near T_C, while for starting temperatures below 163 K, a new anomaly appears. Examination of the dilation curves between 140 and 160 K showed that the temperature position of the anomaly is a linear function of the starting temperature but that the electric field (4.2 V/cm) at which the anomaly appears is independent of the temperature. On raising the starting temperature further, the anomaly at T_C develops eventually into a simple slope discontinuity as shown in Fig. 11. It is interesting to note here that an extra increase in the modulus softening of *o*-TaS_3 below 160 K has been reported by Jacobsen and Mozurkewich.[20] It is not clear, however, whether this modulus anomaly is in any way related to the expansion anomaly observed here. Although the results on the 0.18% strained sample were very reproducible for successive temperature sweeps, an insufficient number of samples have been investigated so far to permit firm conclusions to be drawn.

V. SUMMARY

A tunneling dilatometer was used to measure the thermal expansion near the CDW onset temperatures of three transition-metal compounds. In the layered material 2*H*-$TaSe_2$ the expansion coefficient has a temperature dependence which is very similar to that reported for the specific heat. Although fluctuations are likely to dominate the behavior near T_C, a mean-field examination of the transition nevertheless suggested that the thermal expansion and specific-heat results are also consistent with the Ehrenfest relations as generalized by Testardi. The expansion measurements for the trichalcogenides were performed through electrical self-heating of the samples. The expansion coefficient for $NbSe_3$ showed some temperature dependence and a discontinuity that is consistent with a mean-field phase transition. The dilation measurements in *o*-TaS_3 could only be performed in the presence of electric fields far in excess of the threshold fields. The extracted expansion coefficient showed only a weak temperature dependence and a small mean-field jump of opposite sign to that observed in $NbSe_3$.

ACKNOWLEDGMENTS

We gratefully benefited from several discussions with Wally Geldart and Antony Simpson and we thank Ben Fullerton for the preparation of the samples. The work was supported by grants from the Natural Sciences and Engineering Research Council of Canada.

[1]For reviews, see P. Monceau, in *Electronic Properties of Inorganic Quasi-One-Dimensional Compounds,* edited by P. Monceau (Reidel, Dordrecht, 1985), Vol. 2; G. Gruner, Rev. Mod. Phys. **60**, 1129 (1988).

[2]For a review, see G. Mozurkewich, *Perspectives in Physical Acoustics,* edited by Y. Fu, R. K. Sundors, and P. Sutharothok-Priesmeyer (World Scientific, Singapore, 1992).

[3]T. M. Tritt, M. J. Skove, and A. C. Ehrlich, Phys. Rev. B **43**, 9972 (1991).

[4]D. Maclean, A. Simpson, and M. H. Jericho, Phys. Rev. B **46**, 12 117 (1992).

[5]M. R. Hauser, B. B. Plapp, and G. Mozurkewich, Phys. Rev. B **43**, 8105 (1991).

[6]For a detailed discussion of the dilatometer, see D. Maclean, Ph.D. thesis, Dalhousie University (unpublished).

[7]C. W. Chu, L. R. Testardi, F. J. DiSalvo, and D. E. Moncton, Phys. Rev. B **14**, 464 (1976).

[8]M. O. Steinitz and J. Grunzweig-Genossar, Solid State Commun. **29**, 519 (1979).

[9]L. R. Testardi, Phys. Rev. B **12**, 3849 (1975).

[10]R. A. Craven and S. F. Meyer, Phys. Rev. B **16**, 4583 (1977).

[11]J. L. Feldman, C. L. Vold, E. F. Skelton, S. C. Yu, and I. L. Spain, Phys. Rev. B **18**, 5820 (1978).

[12]G. Brusdeylins, C. Heimlich, J. G. Skofronick, J. P. Toennies, R. Vollmer, and G. Benedek, Europhys. Lett. **9**, 563 (1989).

[13]S. Tomic, K. Biljakovic, D. Djurek, J. R. Cooper, and P. Monceau, Solid State Commun. **38**, 109 (1981).

[14]R. S. Lear, M. J. Skove, E. P. Stillwell, and J. W. Brill, Phys.

Rev. B **29**, 5656 (1984).
[15]Yiqin Wang, M. Chung, T. N. O'Neal, and J. W. Brill, Synth. Met. **46**, 307 (1992).
[16]J. W. Brill, Mol. Cryst. Liq. Cryst. **81**, 107 (1982).
[17]S. Hoen, B. Burk, A. Zettl, and M. Inui, Phys. Rev. B **46**, 1874 (1992).
[18]V. B. Preobrazensky and A. N. Taldenkov, in *Charge Density Waves in Solids,* edited by Gy. Hutiray and J. Solyom (Springer-Verlag, Berlin, 1985), p. 431.
[19]X. D. Xiang and J. W. Brill, Phys. Rev. Lett. **63**, 1853 (1989).
[20]R. L. Jacobsen and G. Mozurkewich, Phys. Rev. B **42**, 2778 (1990).